The 1.1 Å Resolution Crystal Structure of [Tyr^{15}]EpI, a Novel α-Conotoxin from *Conus episcopatus*, Solved by Direct Methods†

Shu-Hong Hu,‡ Marion Loughnan,‡ Russ Miller,§,|| Charles M. Weeks,|| Robert H. Blessing,|| Paul F. Alewood,‡ Richard J. Lewis,‡ and Jennifer L. Martin*,‡

Centre for Drug Design and Development, University of Queensland, Brisbane, QLD 4072 Australia, Department of Computer Science, State University of New York at Buffalo, Buffalo, New York 14260, and Hauptman-Woodward Medical Research Institute, 73 High Street, Buffalo, New York 14203

Received March 20, 1998; Revised Manuscript Received June 8, 1998

ABSTRACT: Conotoxins are valuable probes of receptors and ion channels because of their small size and highly selective activity. α-Conotoxin EpI, a 16-residue peptide from the mollusk-hunting *Conus episcopatus*, has the amino acid sequence GCCSDPRCNMNNPDY(SO_3H)C-NH_2 and appears to be an extremely potent and selective inhibitor of the α3β2 and α3β4 neuronal subtypes of the nicotinic acetylcholine receptor (nAChR). The desulfated form of EpI ([Tyr^{15}]EpI) has a potency and selectivity for the nAChR receptor similar to those of EpI. Here we describe the crystal structure of [Tyr^{15}]EpI solved at a resolution of 1.1 Å using *SnB*. The asymmetric unit has a total of 284 non-hydrogen atoms, making this one of the largest structures solved de novo by direct methods. The [Tyr^{15}]EpI structure brings to six the number of α-conotoxin structures that have been determined to date. Four of these, [Tyr^{15}]EpI, PnIA, PnIB, and MII, have an α4/7 cysteine framework and are selective for the neuronal subtype of the nAChR. The structure of [Tyr^{15}]EpI has the same backbone fold as the other α4/7-conotoxin structures, supporting the notion that this conotoxin cysteine framework and spacing give rise to a conserved fold. The surface charge distribution of [Tyr^{15}]EpI is similar to that of PnIA and PnIB but is likely to be different from that of MII, suggesting that [Tyr^{15}]EpI and MII may have different binding modes for the same receptor subtype.

Conotoxins are small (usually 10−30 residues), cysteine-rich peptides found in the venom of predatory marine snails, *Conus* sp. (*1*). The cone snails immobilize their prey (worms, mollusks, or fish) by envenomation with a highly specialized cocktail of peptide toxins (*2*). There are five major classes of disulfide bond-stabilized conotoxins. These are the α-conotoxins which block competitively the nicotinic acetylcholine receptor (nAChR)[1] (*3*), the ω-conotoxins which block the neuronal calcium channel (*4*), the μ- and δ-conotoxins which block or delay inactivation of the sodium channel, respectively (*1*, *5*, *6*), and the κ-conotoxins which block the potassium channel (*7*). These toxins are utilized as research tools in many fields of neurobiology since they represent high-affinity ligands for a variety of receptors and ion channels critical to the functioning of the neuromuscular system. In addition, the small size of these peptides allows them to be readily synthesized, and they are ideal scaffolds for peptidomimetic design.

The nAChR is a member of the ligand-gated ion channel family of receptors which play a critical role in nerve signal transmission (*8*). The nAChR has been implicated in a variety of neuropsychiatric disorders, including Alzheimer's disease and dementias (*9*). This receptor is found in muscle and neuronal tissues. The muscle-type nAChR is assembled as a heteropentamer comprising the subunits $(\alpha1)_2\beta1\gamma\delta$ in developing muscle and $(\alpha1)_2\beta1\epsilon\delta$ in mature muscle (*10*). The neuronal-type nAChR is also a pentamer but is formed only from α-subunits (of subtypes α2−7 and α9) and β-subunits (subtypes β2−4). Since ion channels are membrane-bound proteins, they are difficult to analyze by either X-ray crystallography or NMR techniques. An alternative approach for studying these receptors is investigation of the high-resolution structures of their ligands such as the highly selective and potent α-conotoxins of interest here.

The α-conotoxins (12−18 residues) are much smaller than snake neurotoxins such as α-bungarotoxin (60−80 residues) which also target the nAChR (*11*). Furthermore, the α-conotoxins can discriminate between subtypes of the nAChR (Figure 1). For example, the muscle nAChR is inhibited by α-conotoxins from fish-hunting cone snails such as *Conus geographus* (GI, GIA, and GII) (*12*), *Conus magus* (MI) (*13*), *Conus striatus* (SI, SIA, and SII) (*14*−*16*), and *Conus ermineus* (EI) (*17*). The neuronal-type nAChR is inhibited by α-conotoxins from mollusk-hunting cone snails such as *Conus pennaceus* (PnIA and PnIB) (*18*) and *Conus episcopatus* (EpI), from worm-hunting cone snails such as

† This work was supported by the Australian Industry Research and Development Board, AMRAD Operations Pty. Ltd., and the Australian Research Council. J.L.M. is supported by a Queen Elizabeth II Fellowship.

* To whom correspondence should be addressed. Phone: +61 7 3365 4942. Fax: +61 7 3365 1990. E-mail: J.Martin@mailbox.uq.edu.au.
‡ University of Queensland.
§ State University of New York at Buffalo.
|| Hauptman-Woodward Medical Research Institute.

[1] Abbreviations: nAChR, nicotinic acetylcholine receptor; HPLC, high-performance liquid chromatography; NMR, nuclear magnetic resonance; rms, root-mean-square.

S0006-2960(98)00654-0 CCC: $15.00
Published on Web 07/25/1998

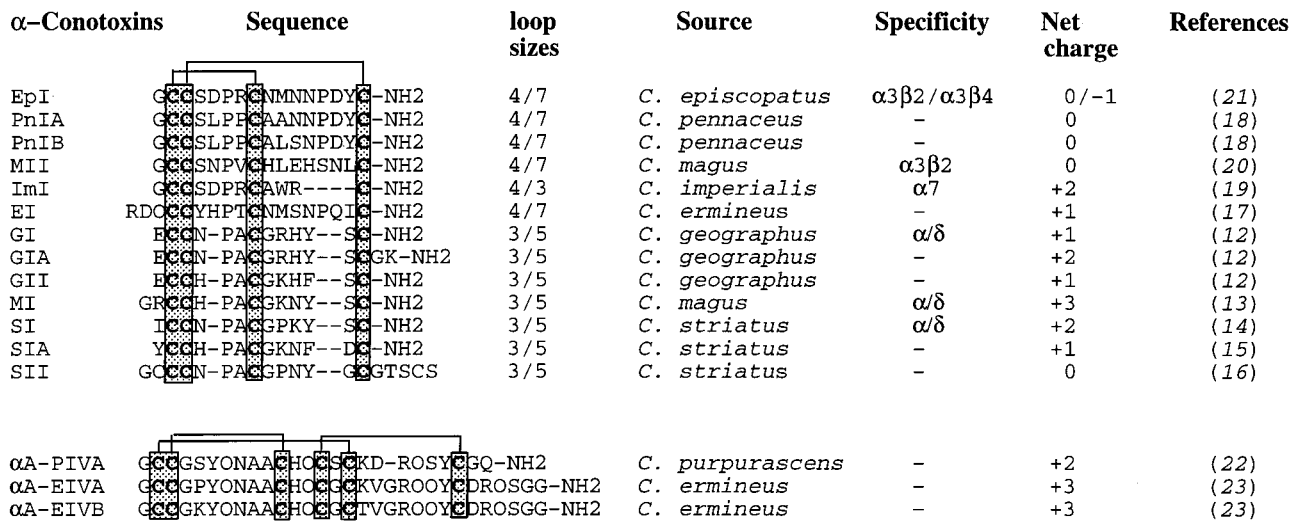

FIGURE 1: Amino acid sequences and conserved cysteine framework (shaded) for the α-conotoxins. The connectivity of the disulfide bonds is shown at the top of the figure (note that α-conotoxin SII has an additional disulfide bond, formed between cysteines 2 and 18, the connectivity of which is not shown). The sequences of the neuronal-selective α-conotoxins are shown at the top, followed by the muscle-selective α-conotoxins (from GI onward). The αA-conotoxins are listed separately. EpI is sulfated at Y15. For the net charge, we assumed positive charges for N termini (where the C termini are amidated), Lys and Arg residues, and negative charges for Glu and Asp residues. NH_2 indicates an amidated C-terminal residue.

Conus imperialis (ImI) (*19*), and from fish-hunting cone snails such as *C. magus* (MII) (*20*). The neuronal α-conotoxins have exquisite selectivity for different receptor subtypes; MII targets specifically the α3β2 receptor subtype (*20*), ImI the α7 homomeric receptor (*19*), and EpI the α3β2 and α3β4 subtype (*21*). A common feature of all α-conotoxin sequences is a two-disulfide linkage pattern, though the size of the loops between the disulfides can vary, giving rise to the α3/5 and the α4/7 classes of α-conotoxins (Figure 1). In addition, the recently identified αA-conotoxins, which also target the nAChR, have a very divergent sequence with a three-disulfide framework (*22*, *23*) (Figure 1).

We have initiated a program of structural studies on the α-conotoxins to investigate the important structural and/or surface features for potency and discrimination between different nAChR subtypes. We have determined the crystal structures of the muscle-selective α-conotoxin GI from *C. geographus* (*24*) and the neuronal selective α-conotoxins PnIA (*25*) and PnIB (*26*) from *C. pennaceus*, and have compared these structures to identify shape and surface charge characteristics that could account for their differing specificities (*26*). Here we report the 1.1 Å crystal structure of the desulfated form of α-conotoxin EpI, a recently identified 16-residue peptide from *C. episcopatus* (*21*) with the sequence GCCSDPRCNMNNPDY(SO_3H)C-NH_2.

EXPERIMENTAL PROCEDURES

Peptide Synthesis, Crystallization, and Data Collection. α-Conotoxin [Tyr^{15}]EpI was synthesized and purified, as described previously (*21*). The purity (>95%) of the peptide was confirmed by analytical reverse-phase HPLC and mass spectrometry. For crystallization, the lyophilized peptide was dissolved in distilled water at a concentration of 15 mg/mL and stored at 4 °C. Large rod crystals of [Tyr^{15}]EpI appeared in this solution within 1 week. These crystals diffract to ~1.1 Å resolution and belong to the tetragonal space group *I*4 with unit cell dimensions $a = b = 44.4$ Å and $c = 23.5$ Å, which is compatible with two molecules of [Tyr^{15}]EpI per asymmetric unit. The crystal volume per unit of molecular mass (V_m) is 1.61 Å^3 Da^{-1} (*27*). The solvent content of the crystals is thus estimated to be 24%, which is similar to that observed for orthorhombic crystals of α-conotoxin PnIB, but twice that of the monoclinic crystals of α-conotoxin PnIA.

Table 1: X-ray Diffraction Data for [Tyr^{15}]EpI

	crystal 1	crystal 2	merged data
maximal resolution (Å)	1.1	2.6	1.1
no. of observations	34402	3604	38406
no. of unique reflections	9101	723	9265
all data			
completeness (%)	95.6	97.0	97.4
R_{sym}[a]	0.072	0.059	0.071
$I/\sigma I$	23.0	43.9	24.9
$I/\sigma I$ (1.1−1.14 Å)	5.3		5.3

[a] $R_{sym} = \Sigma|I - \langle I\rangle|/\Sigma\langle I\rangle$, where I is the intensity measurement for a particular symmetry-related reflection and $\langle I\rangle$ is the average intensity over all symmetry-related reflections.

Data at 1.1 Å resolution were measured from two crystals of [Tyr^{15}]EpI at 16 °C using an R-axis IIC imaging plate area detector system mounted on a Rigaku RU-200 copper rotating anode X-ray source, operating at 46 kV and 60 mA (with a Yale double-focusing mirror monochromator, a 0.2 mm cathode, and a 0.5 mm collimator). The two crystals were used to measure a high-resolution (1.1 Å) and a low-resolution (2.6 Å) shell of data. For the high-resolution data, the detector distance was 93 mm and the swing angle (2θ) was 44°. For the low-resolution data, the detector was set at 137 mm and 0°. The data for the two crystals were processed using DENZO (*28*) and merged before symmetry averaging and scaling with SCALEPACK (*29*). The crystallographic statistics for data measurement are shown in Tables 1 and 2.

Structure Determination by SnB. Normalized structure factor magnitudes (|*E*|'s) were obtained using LEVY/EVAL (*32*). Initial attempts to solve the structure using *SnB*, version 1.5 (*30*), were unsuccessful. It was noticed that many of

Table 2: R_{sym} as a Function of Resolution for the Merged Crystallographic Data

resolution (Å)	R_{sym}	completeness (%)	resolution (Å)	R_{sym}	completeness (%)
20.0−2.37	0.066	97.6	1.39−1.30	0.125	99.3
2.37−1.88	0.066	99.1	1.30−1.24	0.151	98.0
1.88−1.64	0.076	100.0	1.24−1.18	0.180	97.5
1.64−1.49	0.085	99.8	1.18−1.14	0.202	96.1
1.49−1.39	0.095	99.3	1.14−1.10	0.240	87.0

the highest peaks on the electron density maps were located at *I*4 special positions, even for those trial structures having the lowest values for the minimal function. Subsequently, the structure was successfully solved using a prerelease of *SnB*, version 2.0 (C. M. Weeks and R. Miller, unpublished results), which has the capability of eliminating peaks lying within a specified excluded volume surrounding special positions.

The prerelease of *SnB*, version 2.0, was applied under the following conditions. A total of 19 000 triples were generated from the largest 1900 *E* magnitudes between resolution limits of 50.0 and 1.1 Å. One thousand starting structures, each consisting of 100 randomly placed atoms, were generated. Each such trial structure was then subjected to 250 cycles of phase refinement and Fourier filtering. Each instance of Fourier filtering consisted of picking the 50 largest peaks in accordance with new recommendations for peak selection involving larger structures (C. M. Weeks and R. Miller, unpublished results). Each instance of phase refinement consisted of making three complete passes through the set of 1900 reflections, where during each such pass, every phase was subjected to a parameter shift routine which applied a maximum of two 90° phase shifts. The refined phase chosen during this parameter shift procedure was that which yielded the smallest value of the objective function (the minimal function). Finally, each trial structure underwent several cycles of *E* Fourier refinement, during which additional peaks were selected.

After about 670 trial structures were processed, a bimodal distribution of minimal function values, characteristic of situations in which solutions are present, was observed. The solution with the lowest value for the minimal function clearly revealed two fragments corresponding to the two molecules in the asymmetric unit, with the eight highest peaks corresponding to the eight sulfur atoms of the disulfide bridges. The sulfurs of the two solvent-exposed and flexible Met 10 side chains were not located in the list of top peaks, probably due to the higher mobility of these side chains compared with that of the side chains of the disulfide-forming cysteines.

Structure Refinement. The four sulfur atoms corresponding to the two disulfides of the PnIA crystal structure (*25*) were superimposed using INSIGHT II (TMSI) onto the eight sulfur atoms of [Tyr15]EpI located using *SnB*. This gave two molecules (A and B) of PnIA oriented in the tetragonal cell of [Tyr15]EpI. The root-mean-square (rms) deviations between the PnIA model-derived sulfur atoms and the *SnB*-identified sulfur positions were 0.24 and 0.15 Å for molecules A and B, respectively. More than 100 other atoms (76 main chain atoms and 28 side chain atoms) identified from the *SnB* phase solution also corresponded closely to atoms in the two PnIA model structures. The two models of PnIA in the [Tyr15]EpI asymmetric unit were therefore used as the starting point for refinement. The four residues which differ in sequence between PnIA (Leu 5, Pro 7, Ala 9, and Ala 10) and [Tyr15]EpI (Asp 5, Arg 7, Asn 9, and Met 10) were initially modeled as alanine.

Table 3: Crystallographic Refinement Statistics for [Tyr15]EpI

	$F > 2\sigma F$ cutoff	$F > 0\sigma F$
resolution range (Å)	6.0−1.1	20−1.1
no. of reflections	8281	9254
isotropic *R*-factor[a]	0.161	0.173
isotropic *R*-free[b]	0.178	0.185
anisotropic *R*-factor[a]	0.134	
anisotropic *R*-free[b]	0.154	
no. of peptide atoms	242	
no. of solvent atoms	42	
rms for bond lengths (Å)	0.006	
rms for bond angles (deg)	1.4	
rms for dihedral angles (deg)	23.6	
rms for improper angles (deg)	1.3	
average *B*-factor (Å^2)		
all atoms	10.2	
main chain atoms	8.9	
side chain atoms	11.5	
solvent atoms	30.6	

[a] $R\text{-factor} = \sum|F_{obs} - F_{calc}|/\sum F_{obs}$. [b] *R*-free as defined by Brünger (*47*).

The initial crystallographic *R*-factor at a resolution of 1.5 Å for the PnIA model of the [Tyr15]EpI crystal structure was 49.6%, with an *R*-free (calculated from 10% of the data) of 57.9%. Rigid body refinement using X-PLOR 3.1 (*33*) reduced the *R*-factor to 41.9% and the *R*-free to 49.7%. Several rounds of model building in O (*34*) and positional and individual *B*-factor refinement with X-PLOR, using the geometrical parameters of Engh and Huber (*35*), gave an *R*-factor of 22.0% and an *R*-free of 23.4% at 1.5 Å resolution. Noncrystallographic symmetry restraints were not used during refinement. The resolution of the data was gradually increased to 1.1 Å, and alternative side chain conformations (each of half-occupancy) were modeled for Ser 4 in both molecules A and B and Asp 5 in molecule B. There was no electron density associated with the side chain of Arg 7 in molecule A, and this was therefore modeled as alanine.

Water molecules were included where difference electron density showed a peak above 3σ, and the modeled water made stereochemically reasonable hydrogen bonds. A final round of X-PLOR positional and individual isotropic *B*-factor refinement for all 2 × 16 residues and 42 water molecules gave an *R*-factor of 16.1% and an *R*-free of 17.8% for all data with structure factor amplitudes ($F > 2\sigma F$) between 6.0 and 1.1 Å. By comparison, the *R*-factor and *R*-free values calculated from all data between 20 and 1.1 Å are very similar at 17.3 and 18.5%, respectively. SHELXL97 (*36*) was used for anisotropic *B*-factor refinement, giving an *R*-factor of 13.3% with an *R*-free of 15.4% for data ($F > 2\sigma F$) between 6.0 and 1.1 Å. Details of the statistics for the final refined structure are shown in Table 3. The quality and geometry of the model were evaluated using PROCHECK (*37*). Coordinates and structure factors for α-conotoxin [Tyr15]EpI have been deposited with the Brookhaven Protein Data Bank (PDB accession code 1a0m) and will be on hold for 1 year.

The structures of α-conotoxins PnIA [PDB accession code 1PEN (*25*)] and PnIB [PDB accession code 1AKG (*26*)] were

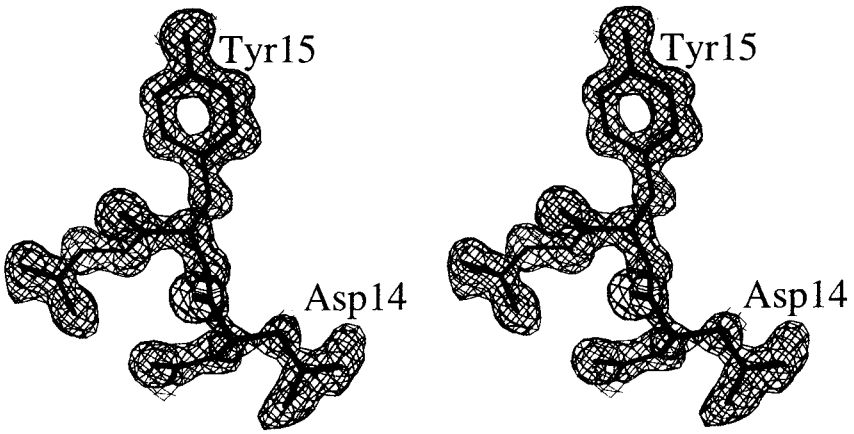

FIGURE 2: Stereoview of the electron density of the $2F_o - F_c$ for the region around residues 14 and 15 of α-conotoxin [Tyr[15]]EpI, contoured at 1σ.

used for structural comparison with [Tyr[15]]EpI. Programs O (*34*), GRASP (*38*), INSIGHT (TMSI), and MOLSCRIPT (*39*), implemented on a Silicon Graphics Indigo R4400 workstation, were used for structural analysis and comparison. Figures for this paper were generated using these programs.

RESULTS

Structure of [Tyr[15]]EpI. The crystal structure of [Tyr[15]]-EpI, which incorporates two molecules (A and B) in the asymmetric unit, was determined by direct methods as implemented in the *SnB* program (C. M. Weeks and R. Miller, unpublished results). The high quality of the final refined model is demonstrated by both the electron density (Figure 2) and the final statistics for X-ray data measurement (Tables 1 and 2) and structure refinement (Table 3). Ramachandran analysis (not shown) of the ϕ and ψ dihedrals of the [Tyr[15]]EpI structure indicates that the backbone dihedrals of all residues fall within the allowed regions. In addition, the mean coordinate error of the structure is estimated to be 0.1−0.25 Å, based on Luzzati plot analysis (*40*) of the crystallographic *R*-factor and *R*-free. The quality of the model is further underlined by the low average isotropic *B*-factors for main chain and side chain atoms of 8.9 and 11.5 Å^2, respectively.

The main feature of the α-conotoxin [Tyr[15]]EpI structure is the two-turn α-helix formed by residues 5−12 (Figure 3). This helix is preceded by a turn comprising residues 2−4: in molecule A of [Tyr[15]]EpI, this turn is classified as a 3_{10}-helical turn, and in molecule B, it is a type I β-turn. At the C terminus of the structure, following the α-helix, there are two consecutive β-turns: residues 12−15 form a type IV turn in both molecules, and residues 13−16 form type IV and type I turns in molecules A and B, respectively.

The structure of [Tyr[15]]EpI is stabilized by two disulfide bridges linking Cys 2 and Cys 8, and Cys 3 and Cys 16, and by a large number of intramolecular hydrogen bonds (28 in molecule A and 24 in molecule B using a 3.4 Å cutoff). In addition, the crystal structure is stabilized by seven intermolecular hydrogen bonds between molecules A and B, 13 crystallographic symmetry-related hydrogen bonds, and ∼60 water-mediated hydrogen bonds. Most of the intramolecular hydrogen bonds in [Tyr[15]]EpI are associated with main chain stabilization of secondary structure elements.

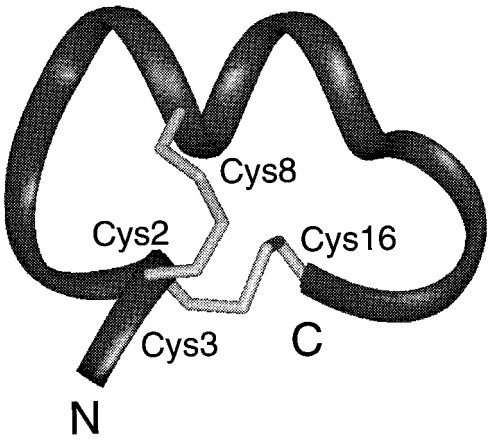

FIGURE 3: Ribbon representation of the α-conotoxin [Tyr[15]]EpI structure with the N and C termini and cysteines of the two disulfide bonds labeled. This figure was produced using INSIGHT.

Intramolecular hydrogen bonds which stabilize side chains of [Tyr[15]]EpI are observed in both molecules A and B for Ser 4 (with main chain atoms of Gly 1), Asp 5 (with main chain atoms of Arg 7 and Cys 8), Asn 9 (with main chain atoms of Cys 3), Asn 11 (with main chain atoms of Arg 7), and Asn 12 (with main chain atoms of Cys 8). In addition, in molecule A, the Ser 4 side chain forms a hydrogen bond to the main chain nitrogen of Asp 5, and in molecule B, a hydrogen bond is formed between the side chain of Asn 12 and the main chain of Asn 11.

Comparison of Molecules A and B of [Tyr[15]]EpI. The two molecules, A and B, in the asymmetric unit of the crystal structure of [Tyr[15]]EpI have similar structures (Figures 4 and 5), with an rms deviation of 0.54 Å for all main chain atoms and 1.17 Å for all atoms. The largest differences between the two structures occur in the C-terminal region of the toxin. If the main chain atoms of three C-terminal residues (13, 15, and 16) are excluded from the main chain comparison, the rms deviation is reduced from 0.54 to 0.37 Å.

For most of the 16 residues, the main chain ϕ and ψ dihedral angles vary by less than 10° between the two structures. The largest variation in main chain angles between the two molecules is 20−30° for Cys 2, Tyr 15, and Cys 16. All four disulfide bridges (Cys 2−Cys 8 and Cys 3−Cys 16 in both molecules of [Tyr[15]]EpI) have the left-handed spiral conformation, which is the most populated disulfide conformation found in protein structures (*41*, *42*).

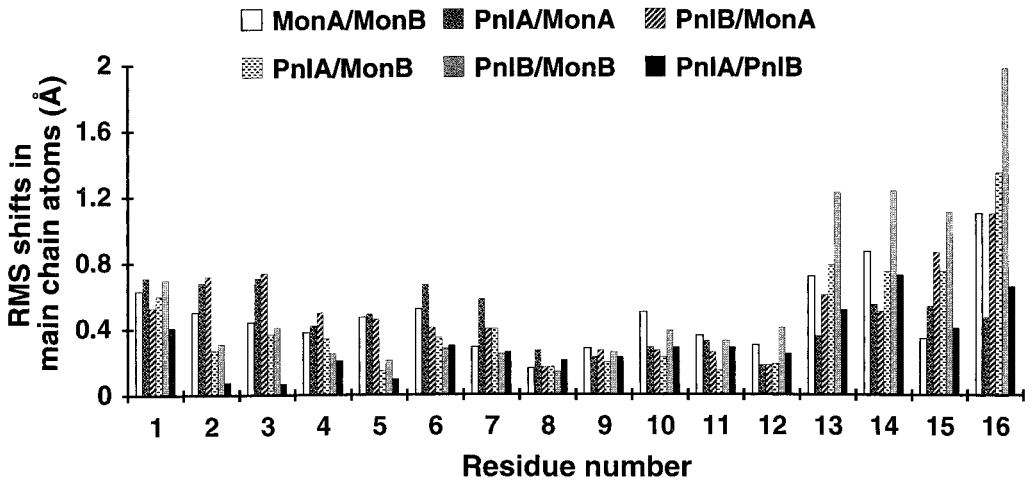

FIGURE 4: Plot of the rms deviations for main chain atoms of each residue for pairs of α-conotoxin crystal structures. The structures compared are (from left to right) (1) [Tyr15]EpI molecules A and B, (2) PnIA and [Tyr15]EpI molecule A, (3) PnIB and [Tyr15]EpI molecule A, (4) PnIA and [Tyr15]EpI molecule B, (5) PnIB and [Tyr15]EpI molecule B, and (6) PnIA and PnIB.

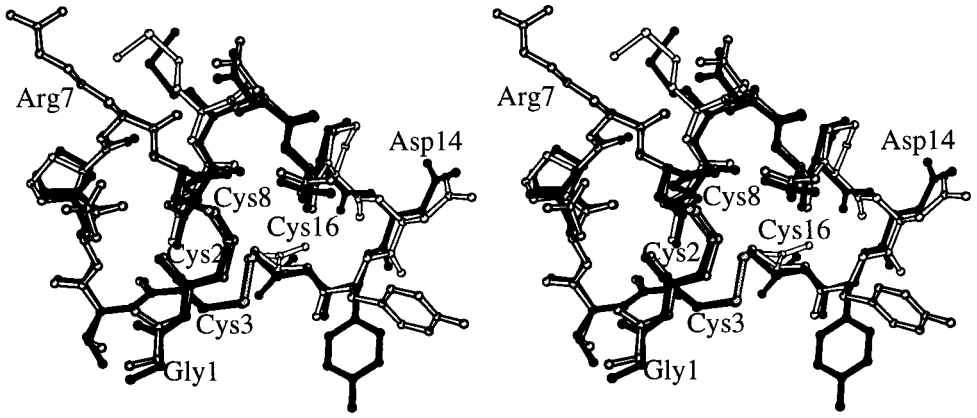

FIGURE 5: Stereoview of the superposition of molecules A (black) and B (white) of the α-conotoxin [Tyr15]EpI in the asymmetric unit. This figure was produced using MOLSCRIPT (*39*).

The presence of two molecules in the asymmetric unit of [Tyr15]EpI is a consequence of crystal packing and is not biologically relevant; under physiological pH, [Tyr15]EpI elutes as a monomer on a size exclusion column (M. Loughnan, unpublished results). In addition, the surface area buried between the two molecules of the asymmetric unit is 254 Å^2 per monomer (using a probe radius of 1.4 Å), corresponding to ~20% of the total accessible surface area per monomer of 1271 Å^2. This buried surface area is much smaller than the values of 26−40% observed for dimeric proteins in the molecular mass range 4−8 kDa (*43*).

The interactions between the two monomers of [Tyr15]EpI are formed primarily through hydrogen bond interactions with the side chains of Asn 12 of molecule A (Asn 12A) and Asp 14 of molecule B (Asp 14B). The side chain of Asn 12A interacts with main chain atoms of Asn 11B, Pro 13B, and Asp 14B (that is, residues from molecule B). The side chain of Asp 14B forms hydrogen bonds to main chain atoms of Asn 12A, Pro 13A, Asp 14A, and Tyr 15A. As a result, the calculated solvent accessibilities of the Asn 12A side chain (<1 Å^2) and the Asp 14B side chain (6 Å^2) are much lower than those of their counterparts, Asn 12B (29 Å^2) and Asp 14A (84 Å^2). The noncrystallographic intermolecular contacts result in a ~10° difference in the side chain rotamer conformation of Asp 14 in the two molecules (Figure 5).

There is a much larger difference between the rotamer conformations of Tyr 15 of molecules A and B (Figure 5). In molecule A, Tyr 15 is in a trans conformation ($\chi_1 = -162°$), but in molecule B, this same residue has a gauche+ conformation ($\chi_1 = -68°$). The conformation of Tyr 15B is stabilized by intermolecular hydrogen bonds to symmetry-related main chain oxygen and side chain Oδ1 atoms of Asn 9B. Tyr 15B cannot adopt the trans conformation observed in molecule A because a steric clash would occur with Pro 13 from a symmetry-related molecule. However, there are no such restrictions for Tyr 15A; it could adopt either the trans or the gauche+ conformation without incurring any unfavorable steric clashes. Since Tyr 15A adopts the trans conformation, this probably better represents the unhindered conformation in solution.

The side chain conformation of Met 10 also differs significantly between molecules A and B (Figure 5). The average separation of equivalent side chain atoms of Met 10A and Met 10B is 1.7 Å. This difference in conformation is probably due to an inherent flexibility of this solvent-exposed hydrophobic residue. The average side chain *B*-factors for Met 10 are 19.4 and 22.2 Å^2 for molecules A and B, respectively, which are much higher than the average value for all side chain atoms in the structure (11.5 Å^2). Furthermore, only one strong van der Waals contact (<3.4 Å) is formed with the side chain of Met 10B (and none for

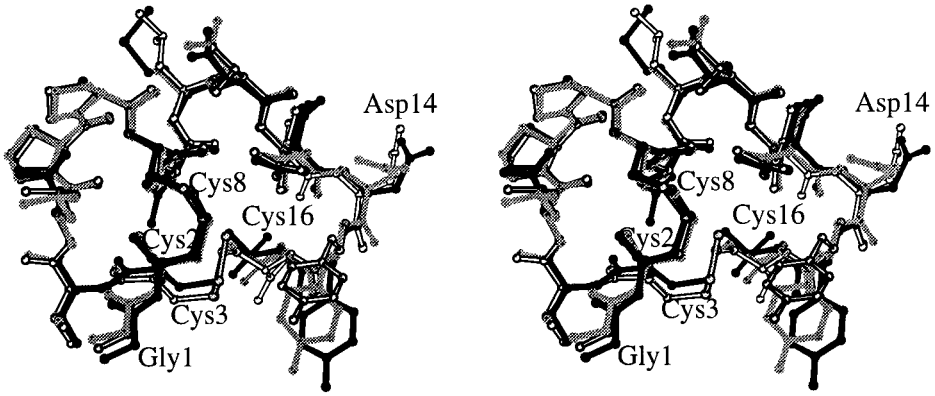

FIGURE 6: Stereoview of the superposition of α-conotoxins [Tyr[15]]EpI molecule A (black), PnIA (gray), and PnIB (white). This figure was produced using MOLSCRIPT (*39*).

Met 10A), though both side chains form four weaker (3.5−4.0 Å) van der Waals contacts.

If the side chain atoms of residues Met 10 and Tyr 15 are excluded from the all-atom comparison of molecules A and B of [Tyr[15]]EpI, the rms deviation is reduced from 1.17 to 0.65 Å.

Solvent Structure. A total of 42 water molecules were modeled into the [Tyr[15]]EpI structure. The average temperature factor (*B*-factor) of these water molecules is 31 Å^2, which is higher than the average *B*-factor of the peptide atoms of [Tyr[15]]EpI (10 Å^2) but similar to the average *B*-factor of waters in the crystal structures of α-conotoxins PnIB (23 waters, average *B*-factor of 27 Å^2) and GI (21 waters, average *B*-factor of 28 Å^2). The average *B*-factor of the waters in the crystal structure of PnIA is somewhat lower (19 Å^2) due to the much lower solvent content (12%) in that crystal form.

The waters in the [Tyr[15]]EpI structure make a similar number of hydrogen bond interactions with each of molecules A and B. Thus, there are 12 and 13 hydrogen bonds between waters and main chain atoms of molecules A and B, respectively, and 16 and 20 hydrogen bonds between water and side chain atoms of molecules A and B, respectively. Of the charged residues in the toxin structure, Asp 5 interacts with two waters in molecule A and three in molecule B. Asp 14A and Asp 14B each interact with one water. The positively charged amino terminus is associated with three waters in molecule A and one water in molecule B. Finally, Arg 7B interacts with five waters (Arg 7A is modeled as Ala in this crystal form). The polar side chains of Ser 4, Asn 9, Asn 11, and Asn 12 interact with one to five waters each. The phenolic hydroxyl group of Tyr 15 in molecule A interacts with two waters (the equivalent hydroxyl in Tyr 15 of molecule B interacts with a symmetry-related Asn 9).

Comparison with Other α4/7-Conotoxin Structures. There are three other published structures of α4/7-conotoxins: PnIA (*25*), PnIB (*26*), and MII (*44*). The coordinates of MII from *C. magus* have not yet been released by the Protein Data Bank so a detailed structural comparison is currently limited to [Tyr[15]]EpI, PnIA, and PnIB. However, the solution structure of MII is described as having the same fold as PnIA (*44*). Comparison of the structures of α-conotoxins [Tyr[15]]EpI, PnIA (*25*), and PnIB (*26*) shows that they all incorporate the same three-dimensional backbone fold (Figure 6).

Superimposition of main chain atoms of [Tyr[15]]EpI with PnIA and PnIB gives an rms deviation of 0.50−0.78 Å. As was found for the comparison of molecules A and B of [Tyr[15]]EpI, the largest differences in structure occur at the C-terminal residues, 15 and 16 especially (Figure 4). If residues 15 and 16 are excluded from the comparison, the rms deviation for all main chain atoms is reduced to 0.4−0.5 Å.

It is noteworthy that even the side chain conformations of [Tyr[15]]EpI are similar to those found for PnIA and PnIB. Thus, Asp 14 adopts the gauche+ conformation in both molecules A and B of [Tyr[15]]EpI and in PnIB. However, in PnIA, the Asp 14 side chain has a gauche− conformation. This is due to a stabilizing hydrogen bond formed between the side chain Oδ2 atom of Asp 14 in PnIA and a symmetry-related main chain nitrogen (*25*). In contrast, the side chains of Asp 14 in molecule A of [Tyr[15]]EpI and PnIB interact only with waters. The side chain of Asp 14B of [Tyr[15]]EpI maintains the gauche+ conformation even though several noncrystallographic intermolecular contacts are formed. Similarly, Tyr 15 adopts a trans conformation in molecule A of [Tyr[15]]EpI and in both PnIA and PnIB. As described above, Tyr 15 in molecule B of [Tyr[15]]EpI cannot adopt the trans conformation because of an unfavorable steric clash with a symmetry-related residue.

DISCUSSION

The structure determination of [Tyr[15]]EpI, with a total of 284 non-hydrogen atoms in the asymmetric unit, represents one of the largest, previously unsolved, structures determined by direct methods (*45*). However, this was not a straightforward process. Initial attempts to solve the structure using *SnB*, version 1.5 (*30*), were unsuccessful. The structure of [Tyr[15]]EpI was solved using a prerelease of *SnB*, version 2.0 (C. M. Weeks and R. Miller, unpublished results). After optimizing parameters for structures in the 1.1−1.2 Å range (*31*), the prerelease of *SnB*, version 2.0, was able to drive 53% of all random trials to solution (for further details, see Experimental Procedures).

The structure determination of [Tyr[15]]EpI brings to six the number of α-conotoxins for which structures are known. Two of these are for muscle-selective α-conotoxins: GI from *C. geographus* (*24*) which has an α3/5 framework and the αA-conotoxin PIVA (*46*) from *C. purpurascens* which has a divergent sequence with three disulfide bonds rather than the usual two. The structures of GI and PIVA differ significantly from each other and from the structures of the

four neuronal selective α-conotoxins which have the α4/7 sequence framework. The α4/7-conotoxin structures are α-conotoxins PnIA (*25*) and PnIB (*26*) from *C. pennaceus*, MII (*44*) from *C. magus*, and now [Tyr15]EpI from *C. episcopatus*.

There are two molecules in the asymmetric unit of the [Tyr15]EpI crystal structure. The two molecules have the same overall fold, which corresponds to the α4/7 fold described previously for the crystal structures of α-conotoxins PnIA and PnIB and the NMR structure of α-conotoxin MII. Comparison of the crystal structures shows that the fold of molecule A of [Tyr15]EpI is as similar to that of PnIA and PnIB (main chain rms deviations of 0.50−0.56 Å) as it is to molecule B of [Tyr15]EpI (main chain rms deviation of 0.54 Å). In contrast, molecule B is the most dissimilar of the structures (main chain rms deviations of 0.54−0.78 Å). PnIA and PnIB are most similar to each other (main chain rms deviation of 0.36 Å). Overall, comparison of the three crystal structures of neuronal-selective α-conotoxins shows that the backbone fold of the α4/7 framework is well-conserved, despite differences in sequence, space groups, crystal contacts, solvent content, and numbers of molecules in the asymmetric unit. The most flexible part of the α4/7 framework is the C terminus (see Figure 4). In the case of [Tyr15]EpI, the C-terminal region of molecule B may be distorted by crystal packing forces (particularly Tyr 15B), but the two independent structures A and B could represent a subset of closely related low-energy conformations sampled in solution.

All four of the α4/7-conotoxins, for which structures are known, selectively block the neuronal subtype of the nAChR. However, the α4/7 framework in itself does not bestow neuronal selectivity since EI, which has the same α4/7 cysteine framework and loop sizes, is selective for the muscle nAChR (*17*). Presumably, the neuronal selectivity of EpI, PnIA, PnIB, and MII resides in the shape and/or surface charge distribution rather than in the backbone fold. We have shown previously that the shape and surface charge distribution of the muscle-selective α-conotoxin GI differ dramatically from those of the neuronal-selective α-conotoxins PnIA and PnIB (*26*); the two neuronal conotoxins are rectangular, and the muscle conotoxin is triangular. In addition, the muscle-specific α-conotoxins typically have a net positive charge and the neuronal-specific α-conotoxins are generally uncharged or have a net negative charge (Figure 1). For example, [Tyr15]EpI has two negatively charged residues (Asp 5 and Asp 14) counterbalanced by Arg 7 and the positively charged N terminus (the C terminus is amidated) giving a net charge of 0. EpI also has a sulfated tyrosine giving a net charge of −1; however, the sulfate is not essential for activity (*21*). Both PnIA and PnIB have one negatively charged residue (Asp 14) counterbalanced by the positively charged N termini to give a net charge of 0. There is some evidence that the tyrosine of PnIA and PnIB may be sulfated (*18*), which would then also give a net charge of −1. The neuronal-selective MII (*20*) has a 0 net charge (Glu 11 and the positively charged N terminus), assuming the two histidines are uncharged at physiological pH. It is tempting to speculate that this difference in net electrostatic charge between the muscle-selective (positive) and neuronal-selective (negative or zero) α-conotoxins may be an important determinant for their differing specificity for neuronal and muscle nAChRs, since electrostatic interactions could allow for molecular recognition over large distances.

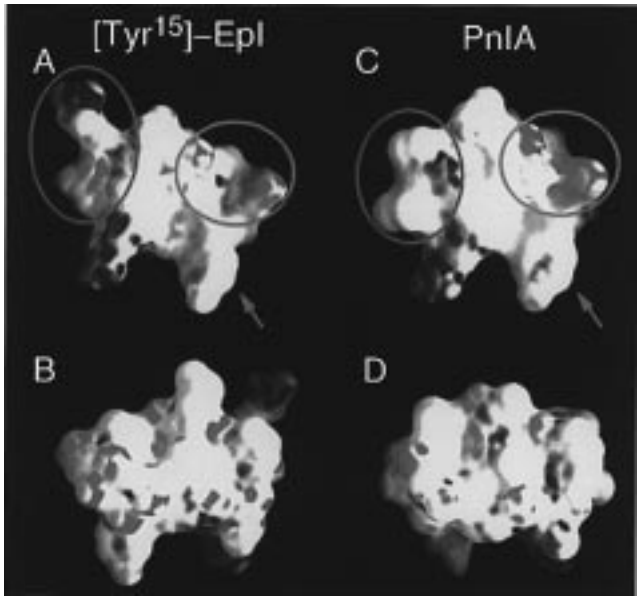

FIGURE 7: Comparison of the electrostatic surfaces of α-conotoxins [Tyr15]EpI (A and B) and PnIA (C and D). For this figure, molecule A of [Tyr15]EpI was used for comparison with PnIA except that the side chain conformation of Arg 7 was modeled from molecule B. The surface is colored according to electrostatic potential: blue for positive, red for negative, and white for hydrophobic regions. The structures in panels A and C are shown in the same orientation as in Figure 3. The structures in panels B and D are views rotated 180° around the vertical axis. The blue circles in panels A and C highlight the regions of [Tyr15]EpI and PnIA with very different electrostatic surfaces. The green arrows in panels A and C identify the tyrosine side chains of [Tyr15]EpI and PnIA. The green circles in panels A and C show the regions that correspond to the hydrophilic surface of MII (*44*). Charges are taken from X-PLOR tophcsdx.pro parameters. This figure was generated using GRASP (*38*).

The neuronal-selective α-conotoxins are able to discriminate between different subtypes of the mammalian neuronal receptor. EpI and [Tyr15]EpI appear to be selective for α3β2 and α3β4 subtypes (21), and MII selectively inhibits the α3β2 subtype (*44*). PnIA and PnIB block neuronal nAChRs in mollusks, but their specificity for mammalian neuronal nAChRs is not known. The surface charge distributions can be compared to identify similarities and differences that could account for variations in activity among the neuronal-selective α4/7-conotoxins. We have shown previously that the surface charge distributions of PnIA and PnIB are virtually identical (*26*); as a result, comparisons and discussions are given here only for PnIA, but these apply equally to PnIB. The surface charge distributions of [Tyr15]EpI and PnIA, shown in Figure 7, are remarkably similar. The only major difference between the two is in the region where two charged residues (Asp 5 and Arg 7) of [Tyr15]EpI are replaced by hydrophobic residues (Leu 5 and Pro 7) in PnIA (circled in blue-green in panels A and C of Figure 7). Given the excellent match between the shape and electrostatic surfaces of [Tyr15]EpI and PnIA, it is plausible that these two molecules could bind in the same manner to the neuronal nAChR and they could share common receptor subtype targets. However, if PnIA and PnIB are shown not to block the same mammalian nAChR subtypes as [Tyr15]EpI, then we can reasonably suppose that residues Asp 5 and Arg 7

are the important discriminators for neuronal nAChR subtype selectivity in [Tyr[15]]EpI since these represent the only major differences in surface and shape.

The α4/7-conotoxin MII is selective for the α3β2 neuronal subtype, so it could be expected to have surface features in common with [Tyr[15]]EpI. The coordinates of MII have not yet been released from the Protein Data Bank, so we are unable to make a direct comparison between the surfaces of MII and [Tyr[15]]EpI. However, the surface features and charge distribution of MII have been described and were shown to be very different from those of PnIA (*44*), using the same backbone orientation. Two regions of the surface of MII were identified as potentially important discriminators for activity. One of the MII surfaces (*44*), described as flat and hydrophobic, is formed by Gly 1 (excluding the positively charged N terminus), Cys 2, Cys 3, Leu 15, and Cys 16. In [Tyr[15]]EpI, PnIA, and PnIB, these residues are the same as in MII, except that Leu 15 of MII is replaced with Tyr 15. The corresponding region in [Tyr[15]]EpI, PnIA, and PnIB is not flat as in MII because the side chain of this tyrosine protrudes from the surface (denoted by arrows in panels A and C of Figure 7). Furthermore, Tyr 15 is sulfated in EpI, and may be sulfated in PnIA and PnIB. Sulfation results in a negative charge, thereby further differentiating this region from the flat hydrophobic surface of MII. The second distinct region on the surface of MII is described as a hydrophilic or highly charged region located almost perpendicular to the flat hydrophobic surface (*44*). This region is formed from residues Glu 11, His 12, Ser 13, and Asn 14 in MII. The corresponding residues in [Tyr[15]]EpI, PnIA, and PnIB are Asn or Ser 11, Asn 12, Pro 13, and Asp 14. Clearly, these residues do form a hydrophilic surface in a region equivalent to that of MII (circled in green in panels A and C of Figure 7), but the distribution of surface charge would be different from that of MII. In addition, the highly charged part of the electrostatic surface of [Tyr[15]]EpI (circled in blue in Figure 7A) would be uncharged in MII (corresponding residues are Asn 5 and Val 7).

These findings show that there are significant differences in hydrophobicity, shape, and charge at three distinct surface regions of [Tyr[15]]EpI and MII. Taken together, the results suggest that these two α-conotoxins are unlikely to interact with the α3β2 neuronal nAChR subtype in the same manner. To effect inhibition of this receptor subtype, [Tyr[15]]EpI and MII could bind in different orientations or at different points on the receptor surface.

In summary, the structure of [Tyr[15]]EpI confirms that the α4/7-conotoxin sequence provides a stable disulfide-bonded framework, upon which the side chains of non-cysteine residues are displayed. We expect that other α-conotoxins having this conserved cysteine framework and spacing will also have this conserved fold. The placement of side chains upon this stable framework produces different surface profiles and charge distributions, which can result in different neuronal receptor subtype specificities. The overall net charge on the α-conotoxin could play an important role in the discrimination between muscle (overall positive charge) and neuronal (overall negative or zero charge) nAChRs.

ACKNOWLEDGMENT

We are very grateful to Prof. Peter Andrews for support and useful discussions. We also thank Trudy Bond for expert technical assistance and John Gehrmann and Justine Hill for helpful discussions.

REFERENCES

1. Olivera, B. M., Rivier, J., Clark, C., Ramilo, C. A., Corpuz, G. P., Abogadie, F. C., Mena, E. E., Woodward, S. R., Hillyard, D. R., and Cruz, L. J. (1990) *Science 249*, 257−263.
2. Kohn, A. J., and Nybakken, J. W. (1975) *Mar. Biol. (Berlin) 29*, 211−234.
3. Olivera, B. M., McIntosh, J. M., Cruz, L. J., Luque, F. A., and Gray, W. R. (1984) *Biochemistry 23*, 5087−5090.
4. Olivera, B. M., Gray, W. R., Zeiku, R., McIntoch, J. M., Varga, J., River, J., de Santos, V., and Cruz, L. J. (1985) *Science 230*, 1338−1343.
5. Fainzilber, M., Nakamura, T., Gathon, A., Lodder, J. C., Kits, K. S., Burlingame, A. L., and Zlotkin, E. (1995) *Biochemistry 34*, 8649−8656.
6. Shon, K.-J., Grilley, M., Marsh, M., Yoshikami, D., Hall, A. R., Kurz, B., Gray, W. R., Imperial, J. S., Hillyard, D. R., and Olivera, B. M. (1995) *Biochemistry 34*, 4913−4918.
7. Terlau, H., Shon, K.-J., Grilley, M., Stocker, M., Stühmer, W., and Olivera, B. M. (1996) *Nature 381*, 148−151.
8. Labarca, C., Nowak, M. W., Zhang, H., Tang, L., Deshpande, P., and Lester, H. A. (1995) *Nature 376*, 514−516.
9. Holladay, M. W., Lebold, S. S., and Lin, N.-H. (1995) *Drug Dev. Res. 35*, 191−213.
10. Galzi, J.-L., Revah, F., Besis, A., and Changeux, J.-P. (1991) *Annu. Rev. Pharmacol. 31*, 37−72.
11. Barchan, D., Ovadia, M., Kochva, E., and Fuchs, S. (1995) *Biochemistry 34*, 9172−9176.
12. Gray, W. R., Luque, A., Olivera, B. M., Barrett, J., and Cruz, L. J. (1981) *J. Biol. Chem. 256*, 4734−4740.
13. McIntosh, J. M., Ghomashchi, F., Gelb, M. H., Dooley, D. J., Stoehr, S. J., Giordani, A. B., Naisbett, S. R., and Olivera, B. M. (1995) *J. Biol. Chem. 270*, 3518−3526.
14. Zafaralla, G. C., Ramilo, C. A., Gray, W. R., Karlstron, R., Olivera, B. M., and Cruz, L. J. (1988) *Biochemistry 27*, 7102−7105.
15. Myers, R. A., Zafaralla, G. C., Gray, W. R., Abbot, J., Cruz, L. J., and Olivera, B. M. (1991) *Biochemistry 30*, 9370−9377.
16. Ramilo, C. A., Zafaralla, G. C., Nadasdi, L., Hammerland, L. G., Yoshikami, D., Gray, W. R., Kristipati, R., Ramachandran, J., Miljanich, G., Olivera, B. M., and Cruz, L. J. (1992) *Biochemistry 31*, 9919−9926.
17. Martinez, J. S., Olivera, B. M., Gray, W. R., Craig, A. G., Groebe, D. R., Abramson, S. N., and McIntosh, J. M. (1995) *Biochemistry 34*, 14519−14526.
18. Fainzilber, M., Hasson, A., Oren, R., Burlingame, A. L., Gordon, D., Spire, M. E., and Zlotkin, E. (1994) *Biochemistry 33*, 9523−9529.
19. McIntosh, J. M., Yoshikami, D., Mahe, E., Nielsen, D. B., Rivier, J. E., Gray, W. R., and Olivera, B. M. (1994) *J. Biol. Chem. 269*, 16733−16739.
20. Cartier, G. E., Yoshikami, D., Gray, W. R., Luo, S., Olivera, B. M., and McIntosh, J. M. (1996) *J. Biol. Chem. 271*, 7522−7528.
21. Loughnan, M., Bond, T., Atkins, A., Jones, A., Gehrmann, J., Cuevas, J., Adams, D. J., Broxton, N., Livett, B., Down, J., Alewood, P. F., and Lewis, R. J. (1998) *J. Biol. Chem. 273*, 15667−15674.
22. Hopkins, C., Grilley, M., Miller, C., Shon, K.-J., Cruz, L. J., Gray, W. R., Dykert, J., River, J., Yoshikami, D., and Olivera, B. M. (1995) *J. Biol. Chem. 270*, 22361−22367.
23. Jacobsen, R., Yoshikami, D., Ellison, M., Martinez, J., Gray, W. R., Cartier, G. E., Shon, K.-J., Groebe, D. R., Abramson, S. N., Olivera, B. M., and McIntosh, J. M. (1997) *J. Biol. Chem. 272*, 22531−22537.

24. Guddat, L. W., Martin, J., Shan, L., Edmundson, A. B., and Gray, W. R. (1996) *Biochemistry 35*, 11329−11335.
25. Hu, S.-H., Gehrmann, J., Guddat, L. W., Alewood, P. F., Craik, D. J., and Martin, J. L. (1996) *Structure 4*, 417−423.
26. Hu, S.-H., Gehrmann, J., Alewood, P. F., Craik, D. J., and Martin, J. L. (1997) *Biochemistry 36*, 11323−11330.
27. Matthew, B. W. (1968) *J. Mol. Biol. 33*, 491−497.
28. Minor, W. (1993) *XDIPLAYF Program*, Purdue University, West Lafayette, IN.
29. Otwinowski, Z. (1993) in *Proceeding of the CCP4 Study Weekend: Data Collection and Processing* (Sawyer, L., Issacs, N., and Bailey, D., Eds.) pp 55−62, SERC Daresbury Laboratory, Warrington, U.K.
30. Miller, R., Gallo, S. M., Khalak, H. G., and Weeks, C. M. (1994) *J. Appl. Crystallogr. 27*, 613−621.
31. Weeks, C. M., and Miller, R. (1997) *Direct methods for solving macromolecular structures*, Kluwer, Dordrecht, The Netherlands.
32. Blessing, R. H., Guo, D. Y., and Langs, D. A. (1996) *Acta Crystallogr. D52*, 257−266.
33. Brünger, A. T. (1992) *X-PLOR (version 3.1) Manual*, Yale University Press, New Haven, CT.
34. Jones, T. A., Zou, J. Y., Cowan, S. W., and Kjeldgaard, M. (1991) *Acta Crystallogr. A47*, 110−119.
35. Engh, R. A., and Huber, R. (1991) *Acta Crystallogr. A47*, 392−400.
36. Sheldrick, G. M. (1997) *SHELXL97, A program for crystal structure refinement*, University of Göttingen, Göttingen, Germany.
37. Laskowski, R. A., MacArthur, M. W., Moss, D. S., and Thornton, J. M. (1993) *J. Appl. Crystallogr. 26*, 283−291.
38. Nicholls, A., Bharadwaj, R., and Honing, B. (1993) *Biophys. J. 64*, 116.
39. Kraulis, P. J. (1991) *J. Appl. Crystallogr. 24*, 946−950.
40. Luzzati, V. (1952) *Acta Crystallogr. 5*, 802−810.
41. Richardson, J. S. (1981) *Adv. Protein Chem. 34*, 1−109.
42. Srinivasan, N., Sowdhamini, R., Ramakrishnan, C., and Balaram, P. (1990) *Int. J. Pept. Protein Res. 36*, 147−155.
43. Janin, J., Miller, S., and Chothia, C. (1988) *J. Mol. Biol. 204*, 155−164.
44. Shon, K. J., Koerber, S. C., Rivier, J. E., Olivera, B. M., and McIntosh, J. M. (1997) *Biochemistry 36*, 15693−15700.
45. Ealick, S. E. (1997) *Structure 5*, 469−472.
46. Han, K.-H., Hwang, K.-J., Kim, S.-M., Kim, S.-K., Gray, W. R., Olivera, B. M., River, J., and Shon, K.-J. (1997) *Biochemistry 36*, 1669−1677.
47. Brünger, A. T. (1992) *Nature 355*, 472−475.

BI9806549